ACS APPLIED BIO MATERIALS

www.acsabm.org Article

Microfluidic Systems with Embedded Cell Culture Chambers for High-Throughput Biological Assays

Arian Jaberi,[⊥] Amir Monemian Esfahani,[⊥] Fariba Aghabaglou, Jae Sung Park, Sidy Ndao, Ali Tamayol,* and Ruiguo Yang*

Cite This: https://dx.doi.org/10.1021/acsabm.0c00439 Read Online

ACCESS | Metrics & More | Article Recommendations | Supporting Information

ABSTRACT: The ability to generate chemical and mechanical gradients on chips is important for either creating biomimetic designs or enabling high-throughput assays. However, there is still a significant knowledge gap in the generation of mechanical and chemical gradients in a single device. In this study, we developed gradient-generating microfluidic circuits with integrated microchambers to allow cell culture and to introduce chemical and mechanical gradients to cultured cells. A chemical gradient is generated across the microchambers, exposing cells to a uniform concentration of drugs. The embedded microchamber also produces a mechanical gradient in the form of varied shear stresses induced upon cells among different chambers as well as within the same chamber. Cells seeded within the chambers remain viable and show a normal morphology throughout the culture time. To validate the effect of different drug concentrations and shear stresses, doxorubicin is flowed into chambers seeded with skin cancer cells at different flow rates (from 0 to 0.2 μL/min). The experimental results show that increasing doxorubicin concentration (from 0 to 30 μg/mL) within chambers not only prohibits cell growth but also induces cell death. In addition, the increased shear stress (0.005 Pa) at high flow rates poses a synergistic effect on cell viability by inducing cell damage and detachment. Moreover, the ability of the device to seed cells in a 3D microenvironment was also examined and confirmed. Collectively, the study demonstrates the potential of microchamber-embedded microfluidic gradient generators in 3D cell culture and high-throughput drug screening.

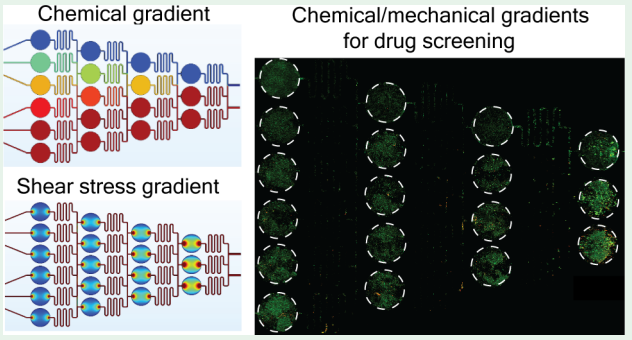

KEYWORDS: *gradient generation, drug screening, shear stress, cell coculture, high-throughput assay*

1. INTRODUCTION

The length scale of microfluidic devices and the availability of many user-defined designs, combined with microfluidic handling capabilities, make them ideal platforms for drug screening[1,2] and microfluidic bioassays.[3] Generation of spatial and temporal chemical gradients in microfluidic devices has been widely reported to study the efficacy and toxicity of drugs[4] and examine their effects on cellular behaviors, such as cell−substrate adhesion,[5] cancer metastasis,[6] angiogenesis,[7] and stem cell differentiation.[8] In addition, versatile gradient generation methods also provide a convenient solution for various immunoassays.[9,10] Moreover, they have been widely adopted in studying bacterial chemotaxis activities.[11−15]

Mixing solutions and generating chemical gradients is an important area that has triggered numerous research activities in microfluidic device design and development. The most common method for generating chemical gradients in microfluidics is by mixing inlet streams containing controlled concentrations of chemicals in microchannels,[16] and one of the common approaches arranges the microchannels in a serpentine shape.[17] By varying the concentration and flow rate of each microchannel inlet, these so-called "Christmas-tree-like" microfluidic networks can generate a profile of chemical gradients at the outlet region.[18,19] This outlet region is normally populated with different types of cells to receive the chemical gradients and to observe the response.[20] These types of devices have been used to study the proliferation and differentiation of neural stem cells,[21] migration of breast cancer cells,[22] colon cancer cells,[23] and toxicity effect of air pollutants on lung cancer cells.[24] Nevertheless, this design has only one culture compartment that can be used to investigate the response of the cultures to chemical gradients. Further, microfluidic devices have been extensively used as high-throughput systems in a way that cellular responses to several conditions can be tested on a single chip.[25,26] However, these high-throughput systems cannot produce different conditions

Received: April 19, 2020
Accepted: July 23, 2020
Published: July 23, 2020

https://dx.doi.org/10.1021/acsabm.0c00439
ACS Appl. Bio Mater. XXXX, XXX, XXX−XXX

automatically and rely on a secondary system for the preparation of the culturing environment.[27]

Microfluidic devices have also emerged as a robust tool for applying mechanical cues to cell cultures.[28] Combining the advances in the fabrication of microfluidic systems and the possibility of incorporation of organoids and tissuelike cultures in a biomimetic environment helped with the realization of organ-on-a-chip and body-on-a-chip platforms. These devices enable studying the effect of drugs, physical, and chemical cues on the viability and functions of cultured cells, tissues, and organoids. For instance, in the study of cancer cells' response to epidermal growth factor (EGF), it has been shown that breast cancer cells respond to mechanical stimuli more evidently than chemical gradients.[29,30] Particularly, the effects of mechanical cues have been reported to exhibit in the form of increased cell mortality and decreased cell adhesion due to increased shear stress. These effects have been shown in prostate cancer cells,[31] breast cancer cells,[32−34] and epithelial ovarian cancer cells.[35] In addition, the effect of shear stress on inducing drug resistance in breast cancer cells has also been demonstrated.[36,37] Thus, it is highly desirable to develop microfluidic chips that can effectively examine the effect of mechanical and chemical stimuli in one single platform.[27,38] Despite the importance of mechanical stimuli in directing cell behavior as discussed above, to date, no robust platform for studying the combined role of chemical and mechanical stimuli on cultured cells has been reported.

In the current study, we extended microfluidic gradient generators to create platforms that can simultaneously generate gradients of mechanical and chemical stresses in a single device. In addition, this chip design utilizes microchambers embedded within channels to provide space for cell culture and exposes these cells to gradients of mechanical shear stress and a chemical treatment. We have effectively proven the efficacy of an anticancer reagent in cancer cells in a dosage-dependent fashion within the microchambers of the device, and more importantly in a synergistic manner with both chemical and mechanical gradients. Finally, this result was confirmed in a viability study in regular dishes. Furthermore, we have demonstrated that this platform can potentially be used for creating cocultures of cells with various ratios. Collectively, this platform will pave the way for drug screening with different stimuli in a controlled 3D microenvironment.

2. RESULTS AND DISCUSSION

2.1. Microchamber-Embedded Gradient Generation Device Design. Considering that microfluidic channels and chambers can also facilitate cell culture and growth, in this study we proposed an innovative design that integrates chemical gradient generation and cell culture in one platform. To this end, microchambers for seeding cells and for drug testing on cultured cells were designed and placed after each serpentine channel of the Christmas-tree-like design. In another design, micropillars were also built into chambers to produce a gradient within the chambers. This integration of microchambers enables the screening of chemical gradients in controlled individual chambers and thus provides a potential method for high-throughput screening of chemical compounds. In addition, this design also allows for the coculture of different cell types at controlled ratios.

Figure 1a,b shows the integrated platform with the microchambers placed after the serpentine microchannels, referred to as a microchamber-embedded Christmas tree (MECT). As illustrated in Figure 1a, each microchamber has different chemical concentrations with the combination of two different media solutions at the two inlets; in the meantime, the concentrations within each microchamber are uniform. To produce a gradient within a microchamber, micropillars are built within each chamber to create a mixing effect and a nonuniform chemical concentration, as illustrated in Figure 1c. In this design, so-called micropillar-embedded microchambers (MPEMs), the micropillar arrays form a network of flow resistors to generate gradients. The microchambers for both devices are designed to be 1 mm in diameter to accommodate about 1000 cells. These dimensions are also tailored to generate shear stresses on the order of 2−10 Pa at the bottom of the chamber as a mechanical stimulus for live cells (to be discussed in the following sections). Figure 1b,d shows the SEM images of the PDMS chips fabricated by soft lithography for the MECT and the MPEM designs, respectively. In addition, the inset for Figure 1b shows the dimension of the serpentine channel, and the inset of Figure 1d shows the dimension of the micropillar array (with a diameter of ∼80 μm for each pillar). It is worth mentioning that the diameter of the micropillar may have an impact on fluid mixing and gradient generation within the chamber. The current design is mostly determined by the limitations of features aspect ratio on the ease-of-peel-off of PDMS microfluidic chips from the silicon mold.

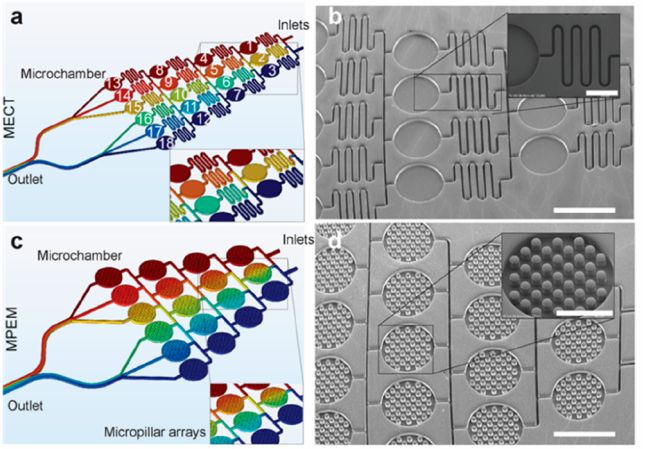

Figure 1. Designs of a microchamber-embedded microfluidic device for gradient generation and drug screening. (a) COMSOL simulation of a microchannel-embedded Christmas tree (MECT) design in which microchambers are embedded after each serpentine microchannel. The gradient is generated across chambers, and uniform concentration is achieved for each chamber. The chambers' number based on their position is demonstrated on each microchamber. (b) SEM images of the entire chip with insets showing the serpentine channel and the microchamber. (c) COMSOL simulation of the micropillar-embedded microchamber (MPEM) design. An overall gradient across chambers as well as a local gradient within each chamber are generated. (d) SEM images of the entire chip with inset showing the chamber and the micropillars. Scale bars: (b) 1000 μm; (b inset) 500 μm; (d) 1000 μm; (d inset) 500 μm.

2.2. Chemical Gradient Generation with Embedded Microchambers. We next investigated the capability of the microchamber-integrated microfluidic devices in generating tunable chemical gradients across chambers and within chambers in MECT and MPEM designs, respectively. This was demonstrated both experimentally and computationally with three different flow rate combinations at the two inlets

https://dx.doi.org/10.1021/acsabm.0c00439
ACS Appl. Bio Mater. XXXX, XXX, XXX−XXX

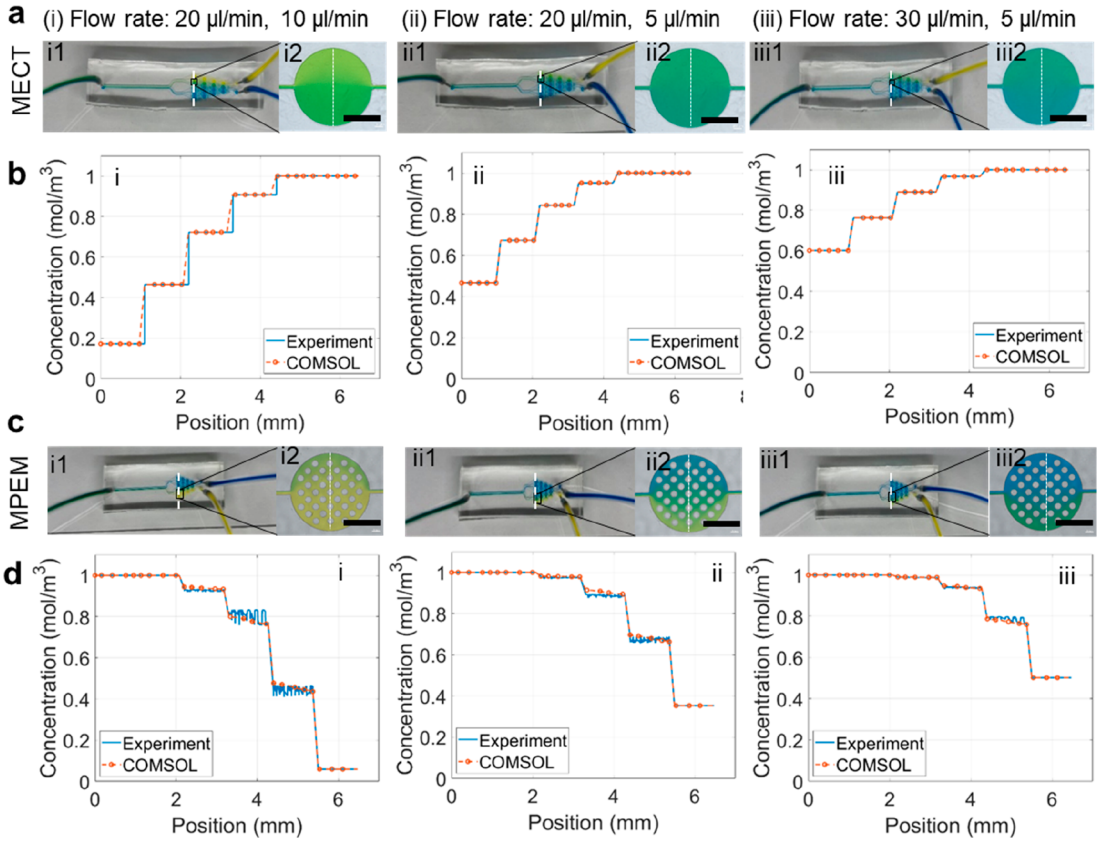

Figure 2. Gradient generation with the MECT and MPEM microfluidic ~~channels.~~ (a) Testing ~~and modeling~~ of the MECT device in generating gradients with different ratios of flow rates at the inlets. The inlets were perfused with media of two different colors, yellow and blue. Three different velocity ratios were shown: 20/10 μL/min (shown in column i), 20/5 μL/min (shown in column ii), 30/5 μL/min (shown in column iii). For each flow rate, the device with the gradient is shown in 1; a zoom-in image of a representative chamber (14) is shown in 2. It is evident that variation in flow rate ratios modifies the chemical gradient produced. (b) The comparison of the experimental data and the simulation data for gradient generation is shown at three flow rate combinations in i−iii. The gradient is captured with the RGB coloration of each chamber. The plot shows the blue color index for the center line of the last column of the device (chambers 13−18) normalized within 0 and 1. (c) Similar to part a, the experiments were conducted for the MPEM device at three different flow rate combinations: i−iii. (d) A comparison of the MPEM device in gradient generation from the experiments and the simulation is shown. Gradient was produced across chambers and within chambers. Scale bars: 500 μm.

from top to bottom: 20 and 10 μL/min (column i), 20 and 5 μL/min (column ii), and 30 and 5 μL/min (column iii). The color gradients for other flow rate combinations where one inlet flow rate was controlled to be constant are shown in Figures S1 and S2 of the Supporting Information.

f2 For the MECT design shown in Figure 2a (i1, i2, ii1, ii2, iii1, iii2), experimentally, solutions with yellow and blue colors were flowed into the inlets at the designated flow rates above. Chemical gradients across all chambers in the four columns, denoted by the difference in color balance, were evident for all three flow rate combinations. In the COMSOL simulation shown in Figure S3a (i−iii), one chemical solution containing 1 mol/m^3 of a chemical species serves as the input to one of the inlets and zero concentration was delivered to the other inlet at the same designated flow rate combinations. A gradient of concentrations was evident for each flow rate combination. Moreover, images of the last six chambers were captured and processed to produce a blue color profile across the center line of the chamber. This color profile was normalized and plotted against the COMSOL simulation data in Figure 2b. An excellent agreement was observed for three flow rate combinations, and different ranges of chemical concentration can be realized with the three flow rate combinations [0.2−1 mol/m^3 in Figure 2b (i), 0.5−1 mol/m^3 in Figure 2b (ii), 0.6−1 mol/m^3 in Figure 2b (iii)].

For the MPEM design shown in Figure 2c, with the same experimental process, a chemical gradient can be produced across different chambers as well as within the individual chambers. These results also agree with the COMSOL simulation data for all flow rate combinations, with the blue color profile from experiments plotted against the concentrations from the simulation for the last six chambers. Specifically, the chemical gradient within each chamber is in a narrower range as compared to the gradients across different chambers. The zoom-in images for the last chamber are shown in Figure 2a,c (i2, ii2, iii2). It is worth mentioning that both devices were designed to be symmetric and were demonstrated as such.

2.3. Mechanical Gradient Generation with Embedded Microchambers. Our COMSOL simulation of the MECT device showed that the amount of shear stress at the bottom of the microchambers, which led to morphological and physiological changes, correlates with the flow rate at the inlets of the microfluidic channel, as demonstrated by the increase of flow velocity and shear stress from a flow rate of 0.1 to 0.2 μL/min (Figure 3a−c to 3d−f). In addition, shear stress f3

https://dx.doi.org/10.1021/acsabm.0c00439
ACS Appl. Bio Mater. XXXX, XXX, XXX−XXX

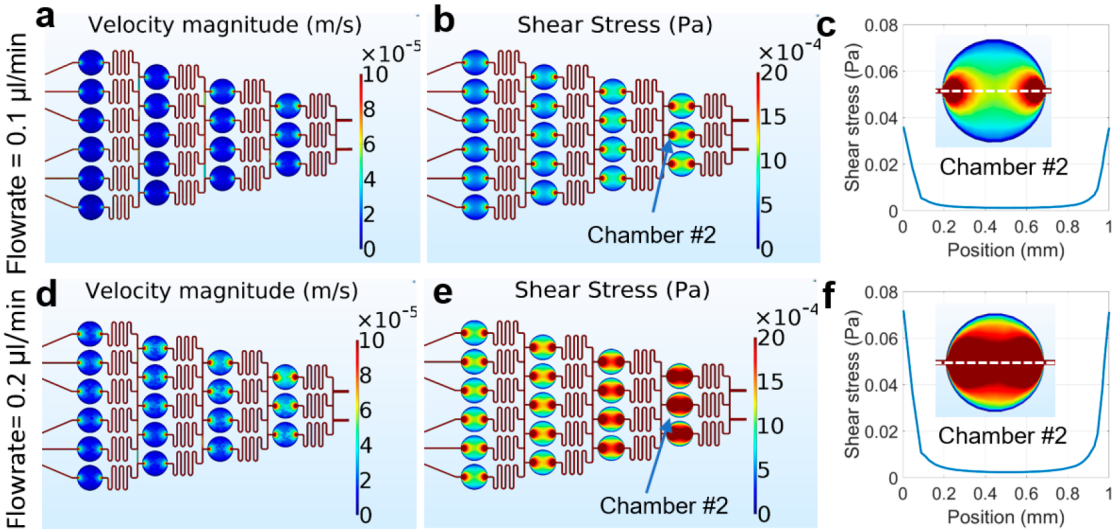

Figure 3. Shear stress analysis of the microchip at two flow rates. (a) Velocity magnitude of the microchip at 0.1 μL/min flow rate shows a symmetric distribution with higher magnitudes within the channels and corners compared to the chambers. (b) Shear stress values of the microchip at 0.1 μL/min flow rate 5 μm from the surface show the same trend as the velocity magnitude. The distribution of shear stress is symmetric. (c) Shear stress distribution inside a representative chamber 2 along the drawn line shows that the shear stress is at its maximum near the entrance and exit of the chamber and is at its minimum in the center of the chamber. (d) Velocity magnitude for 0.2 μL/min also shows the same trend as 0.1 μL/min flow rate. (e) Shear stress distribution along the center line of the chamber for 0.2 μL/min compared to 0.1 μL/min shows higher values of shear stress with the same distribution. (f) Shear stress values along the symmetry line in chamber 2 are shown.

decreased significantly from the chambers in the columns close to the inlets (1, 2, and 3) to the chambers close to the outlet (13, 14, 15, 16, 17, and 18) due to changes in the frontal cross-sectional area per column and the flow rate per column of chambers. Further, shear stress within the chamber was higher closer to the inlet and outlet of the chamber, as shown by the cross-section of the shear stress distribution within chamber 2 for both flow rates (Figure 3c,f). Note that the amplitude of the shear stress produced by the selected flow rates is captured 5 μm above the bottom surface of the chamber. This is about the thickness of a cell, and the values represent the shear stress exerted on cell surfaces. With an average of 0.005 Pa for the 0.2 μL/min flow rate, the shear stress amplitudes fall within the normal physiological conditions.[39,40] It is worth mentioning that the relative flow rate ratio at the two inlets determines the chemical gradients within the microchambers as demonstrated in Figure 2, while the absolute values of flow rates determine the amplitude of the shear stress as shown here in Figure 3.

2.4. Effect of Chemical and Mechanical Gradient on Cell Viability. We next examined the effect of drug concentration and flow-induced shear stress on cells seeded within the microchambers. We initially cultured cancer epithelial cells A431 at the concentration of approximately 580 cells/well. The cultures were then treated with doxorubicin (Dox), a commonly known chemotherapy drug blocking the topoisomerase 2 enzyme in cancer cells to stop cancer cell growth.[41] We examined the difference in cell viability for different dosages of Dox across microchambers in the device. These data were later compared with studies conducted in Petri dishes for confirmation. Considering the effect of flow-induced shear stress exerted upon cells from the microfluidic flow, we further examined the efficacy of Dox in combination with shear stress.

Taking advantage of the ability of the MECT device in generating a uniform gradient within each chamber, we performed a drug screening study with A431 cells administrated with control media and Dox. We studied four conditions in Figure 4: (1) Cells were stained with a live/dead assay 24 h after seeding without any media flow. This serves as the control. (2) Cells were perfused by Dulbecco's modified Eagle's medium (DMEM) from both inlets for 12 h before live/dead staining at a flow rate of 0.1 μL/min. This experimental condition examined the effect of shear stress on cell viability. (3, 4) Cells were perfused for 12 h with Dox in DMEM solution (at a concentration of 30 μg/mL) from the bottom inlet and DMEM only from the top inlet at flow rates of 0.1 μL/min (3) and 0.2 μL/min (4) for both inlets. Representative images for the studies of conditions 1−4 are shown in Figure 4a−d. These studies were performed after the cells had been seeded within the microchambers for 24 h. In addition, cells were perfused with the same condition as 3 and 4 but at the flow rate of 0.05 μL/min, and the representative images of this condition are shown in Figure S4.

Live/dead assay staining without fluid flow showed that cells were attached with well-spread morphology across chambers (zoom-in images for individual chambers in Figure S5 in the Supporting Information) (Figure S6), with high viability of an average of 95% for all chambers as shown in Figure 4a (i) (live cells in green) and Figure 4a (ii) (dead cells in red). This provided clear evidence that cells within each chamber were viable, and the device works properly. The effect of shear stress was then examined by perfusion of both inlets with a control media, DMEM, at a flow rate of 0.1 μL/min. Overall, slightly lower cell viability, at an average of 88%, was observed due to shear-induced cell death [Figure 4b (i) and 4b (ii)]. In addition, the cell viability increased from the columns closest to the inlet of the device to the columns closest to the outlets [Figure 4b (i)], in agreement with the COMSOL simulation where the shear stress is higher in the columns close to the inlets (Figure 3).

Flowing Dox in combination with DMEM at the inlets produced a chemical gradient of Dox across chambers as expected, and this concentration gradient clearly induced different cell viability across chambers. For both flow rates of

https://dx.doi.org/10.1021/acsabm.0c00439
ACS Appl. Bio Mater. XXXX, XXX, XXX−XXX

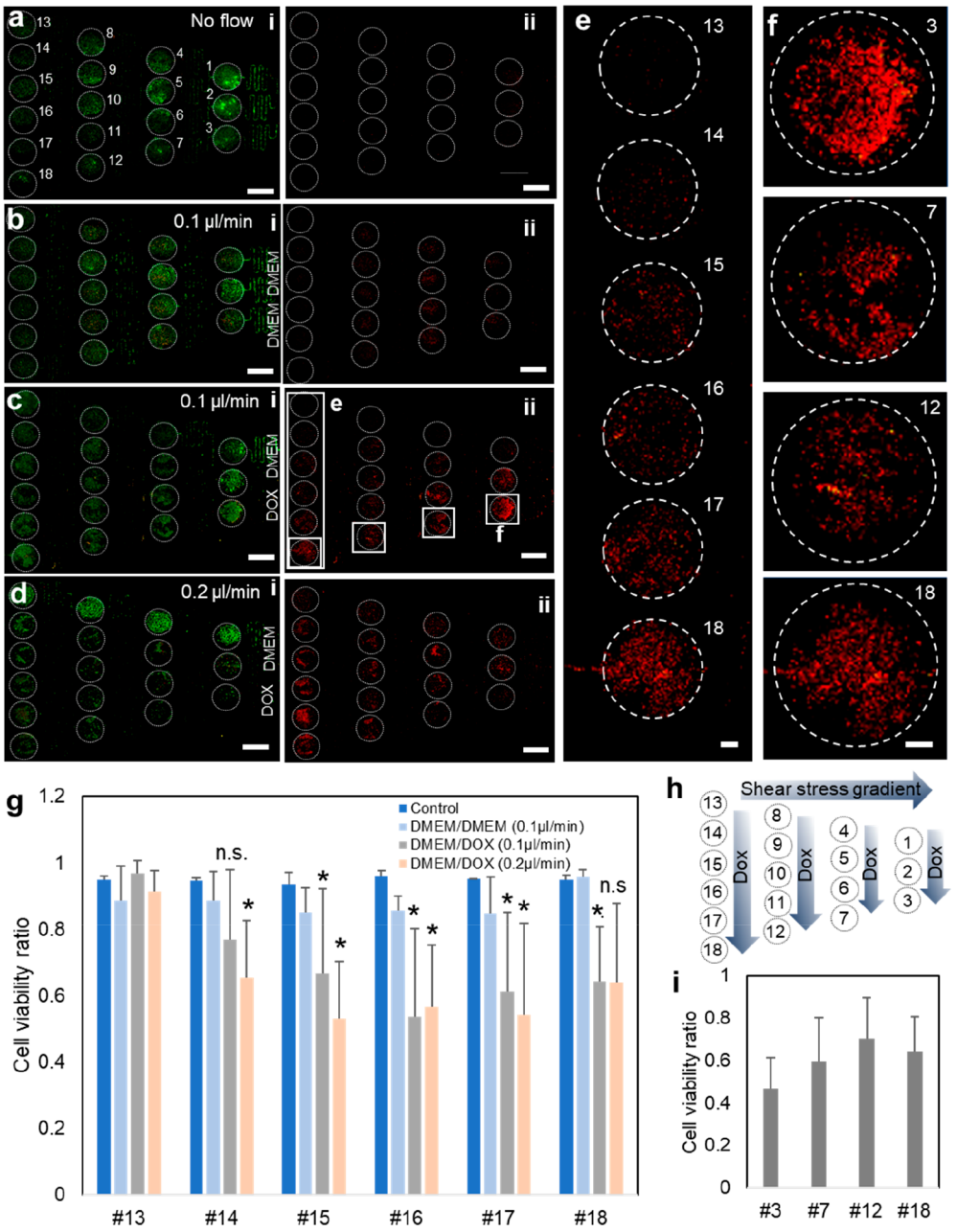

Figure 4. Drug screening treatment on A431 cells using the microfluidic device. Four testing conditions were shown: (a) Cells were stained with a live/dead assay 24 h after seeding as control. (b) Cells were subject to 12 h of flow of DMEM from both inlets before live/dead staining. (c, d) Cells were subject to 12 h of flow of DMEM/Dox (at a concentration of 30 μg/mL) (DMEM for the top inlet, DMEM/Dox for the bottom inlet) at flow rates of 0.1 μL/min (c) and 0.2 μL/min (d) for both inlets. For each condition, composite images for live/dead cells (green and red) are shown in i, and the dead cells (red) are shown in ii. (e) Zoom-in image from the fluorescent image of the dead cells of the first column (chambers 1−3) for the 0.1 μL/min DMEM/Dox condition, showing the increase in the number of dead cells. (f) Zoom-in images from chambers 3, 7, 12, and 18 for the 0.1 μL/min DMEM/Dox condition, showing the increase in the number of dead cells. (g) Cell viabilities in the last column of the chambers in the microfluidic device are shown for no flow, 0.1 μL/min DMEM/DMEM, 0.1 μL/min DMEM/Dox, and 0.2 μL/min DMEM/Dox. (h) Illustration of chemical gradient and shear stress gradient across different chambers of the four columns. (i) Cell viability from the chamber 3, 7, 12, and 18 in DMEM/Dox 0.1 μL/min condition. Scale bars: (a−d) 1000 μm, (e) 200 μm, (f) 100 μm. *: $p < 0.05$ compared with chamber 13 in the same conditions.

0.1 and 0.2 μL/min, cell viability decreased significantly from the top chamber of each column, where the Dox concentration is the lowest, to the bottom chamber of each column, where the Dox concentration is the highest (Figure 4c,d). In particular, representative images in Figure 4e show a group of zoom-in images of the live/dead staining for chambers 13−18 in condition 3 (0.1 μL/min DMEM/Dox), clearly demonstrating an increase in the number of dead cells from 13 to 18 with an increase of Dox concentration. A quantitative data set summarizing all four conditions in five replicates in Figure 4g shows the overall decline of cell viability from chambers 13 to 18 for the two flow rates with DMEM/Dox combination (conditions 3 and 4), significantly different from the controls, while the cell viability remains stable for control

https://dx.doi.org/10.1021/acsabm.0c00439
ACS Appl. Bio Mater. XXXX, XXX, XXX−XXX

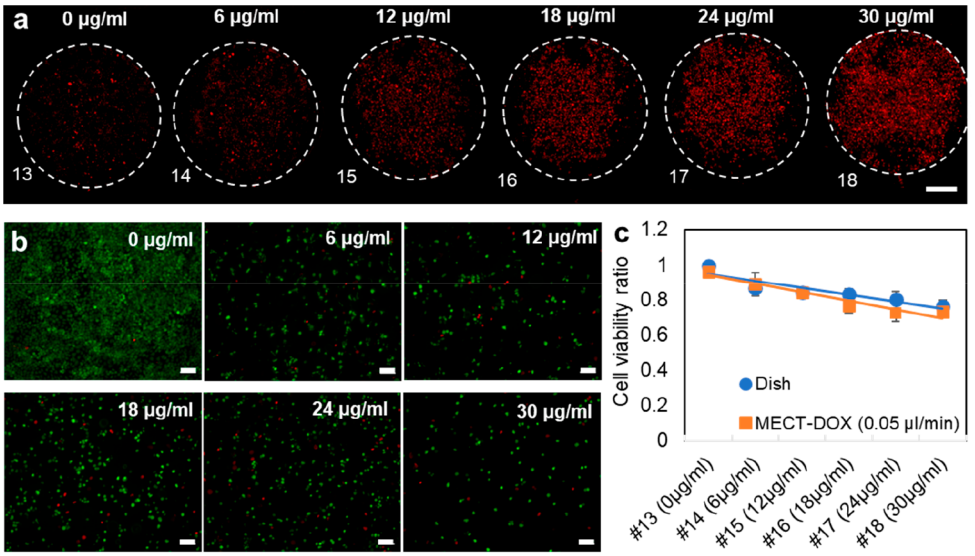

Figure 5. Comparison of cell viability with multiwell dish study and microfluidic device study. (a) Fluorescent images of the stained dead cells in the 0.05 μL/min DMEM/Dox condition from the last column of chambers, from chamber 13 to 18, are placed left to right in this panel. (b) Fluorescent images from the multiwell Dox study on A431 cells with different concentrations of the Dox: 0, 6, 12, 18, 24, 30 μg/mL, matching the concentration in microchambers 13−18. (c) Cell viabilities within the chamber of the last column of the microfluidic device in the 0.05 μL/min DMEM/Dox condition are compared with cell viability of the multiwell study with the same concentrations. Scale bars: (a) 200 μm; (b) 100 μm.

with no flow and for DMEM only at 0.1 μL/min (both inlets) flow rate (condition 1 and 2). Some of the larger error bars in Figure 4i plots may be due to the difference in cell confluency before the drug test experiments due to the difference in the number of cells seeded in the chambers throughout different trials. Dox is not affecting cellular secretome, and the used cells are not known to use secretomes for signaling; therefore, it is expected that cells will not be affected by the upstream culture, but for the sensitive cells and processes, cells can be cultured in one column of the chambers to avoid the upstream secretome interferences.

Flow-induced shear stress gradient alone induced a non-significant change in cell viability, comparing the viability data from condition 2 to condition 1 (Figure 4g). However, we observed a synergistic effect between the drug treatment and shear stress from the overall cell viability and the patterns of cells attached within individual chambers after drug treatment. First, due to the higher shear stress produced from a higher flow rate in condition 4 (0.2 μL/min DMEM/Dox), the overall cell viability in condition 4 is clearly lower than that in condition 3 (0.1 μL/min DMEM/Dox), shown in the representative images in Figure 4c,d as well as the quantitative data in Figure 4g. Second, within a single testing chip, as illustrated in Figure 4h, shear stress increases in columns of chambers close to the inlet, while Dox concentration increases in each column from the top chamber to the bottom chamber. Significant cell death induced by a combined effect of shear stress and drug treatment can be observed in chambers with higher Dox concentration and with higher shear stress, for instance, comparing chambers 3, 7, 12, and 18 in condition 3 (Figure 4i), also shown in the representative images in Figure 4f. It is worth mentioning that the viability number of those chambers in condition 4 may have been skewed by the high detachment rate due to the higher levels of flow-induced shear stress. Lastly, there is a clear pattern of flow-induced cell detachment, in chambers 4−7 in Figure 4c (i) and chambers 13−18 in Figure 4d (i), and the pattern shows an agreement with the simulation data in Figure 3c, where regions of higher shear stress have fewer attached and living cells. It is also worth mentioning that the cell study was carried out on the MECT chips, given the similar shear stress profile (Figure S8); we expect a similar outcome using the MPEM chips. In addition, the small concentration gradient within the chamber of MPEM can be useful in studies involving sensitive biological assays, such as growth factor stimulation.

2.5. Comparison between the Microfluidic Devices with a Petri Dish in a Drug Study. The effect of the Dox concentration on cell viability across different chambers was confirmed by a comparative study with drug tests in a Petri dish. Viability data with DMEM/Dox at the inlets at a flow rate of 0.05 μL/min were compared with the Dox treatment of A431 cells in static culture. A lower flow rate was chosen to minimize the effect of the shear stress on cell detachment and cell death. Representative images of live/dead staining after DMEM/Dox flow for the last column (chambers 13−18) are shown in Figure 5a. Cell viability data were collected by counting cells stained green and red from these chambers. According to simulation data, the concentration of Dox in chambers 13−18 are 0, 6, 12, 18, 24, and 30 μg/mL. These concentrations were applied in static culture, and the viability data were collected. Representative images of static culture treated with Dox of different concentrations are shown in Figure 5b and Figure S7 of the Supporting Information. The quantitative data presented in Figure 5c for both studies showed reasonable agreement, verifying the effectiveness of the device in drug screening.

The proposed chip provides a platform where not only screening of drug dosages can be performed in high throughput on small microchambers, but also the synergistic effect between mechanical stimulants and chemical compounds can be explored in a dosage-dependent manner. The chemical gradients, produced in chambers in the same column, and the shear stress gradient, generated due to microfluidic flow across different columns from the inlet to the outlet, create a matrix of

https://dx.doi.org/10.1021/acsabm.0c00439
ACS Appl. Bio Mater. XXXX, XXX, XXX−XXX

chambers where the effect of different combinations of chemical and mechanical treatments can be examined. This concept is illustrated in Figure 4h, where arrows point in the direction of increasing shear stress and chemical concentration, and our anticancer studies clearly demonstrated that the increase in dosage and in shear stress synergistically enhanced higher cell death rate. This capability can be considered a step forward as compared with devices that only test the effect of chemical gradients on organoids and cell cultures[42,43] or studies that only examine the effect of shear stress on cancer cells.[36,37] It should be noted that the number of chambers can be expanded to include more concentrations, while the shape of the microchamber can be modified to produce different shear stress profiles. Further, the microchambers can be tethered at the bottom onto additional PDMS layers separated by a thin porous membrane to introduce additional stimulants, such as other chemical compounds or oxygen.[44−46] This transparent system is compatible with microscopes for on-line imaging from the individual chambers, in which immunostaining of the cultured cells can be used for biological assays. In addition, the size of the chambers allows electrochemical sensors to be embedded for monitoring the environment and functionality of the cultured cells.

2.6. 3D Cell Seeding and Cell Culture within Embedded Chambers. In newly developed microfluidic devices, the traditional 2D cell culture practices have given way to 3D cell culture schemes to closely recapitulate the microenvironment in vivo.[47] 3D cell culture platforms allow for omnidirectional cellular growth with biomimetic cell−cell and cell−extracellular matrix (ECM) interactions.[48] The 3D cell culture using hydrogels,[49] fibrous scaffolds,[50] and droplet suspensions[51] within microfluidic devices has demonstrated different drug responses, cell morphologies, and proliferation patterns than static 2D cell cultures.[52] Microfluidic systems have also been utilized for creating cellular patterns in 2D and 3D environments.[53−55] These devices have shown great promise for depositing cells in a highly defined fashion and over a scale of several centimeters. Despite this progress, the capability of such systems for engineering coculture of different cells is not well-explored, especially considering the potential of cocultures exposed to different drug compounds.

In this study, we explored the capability of the microchamber-based device in 3D cell culture. In drug screening, current microfluidic devices allow only one controlled area for cell seeding and interaction with the chemicals. Our goal was to introduce spaces within the channels which serve as reaction chambers, and cells seeded within each chamber receive different dosages of the chemicals, paving the way for high-throughput drug screening. Furthermore, this design provides a means to seed different cell types for coculture, affording new potentials of screening cell−cell interactions. To this end, two types of cells were encapsulated in 7% (w/v) gelatin methacryloyl (GelMA) solution, a widely used hydrogel for encapsulating the cells, containing photoinitiator (PI) at a concentration of 0.1% (v/v) that could be cross-linked in situ to provide a 3D microenvironment. This particular concentration is optimized as shown in Figure S9. This concentration of GelMA has been successfully used for long-term 3D culture of various cells.[56] The GelMA solution was then flowed into the inlets of the MECT and MPEM devices at controlled flow rates. Once a steady flow condition was achieved, the solution flow was stopped, and a UV light was applied onto the microchambers through a mask to cross-link GelMA. Cross-linked GelMA encapsulated cells in a 3D environment within each microchamber. This process is illustrated in Figure 6a.

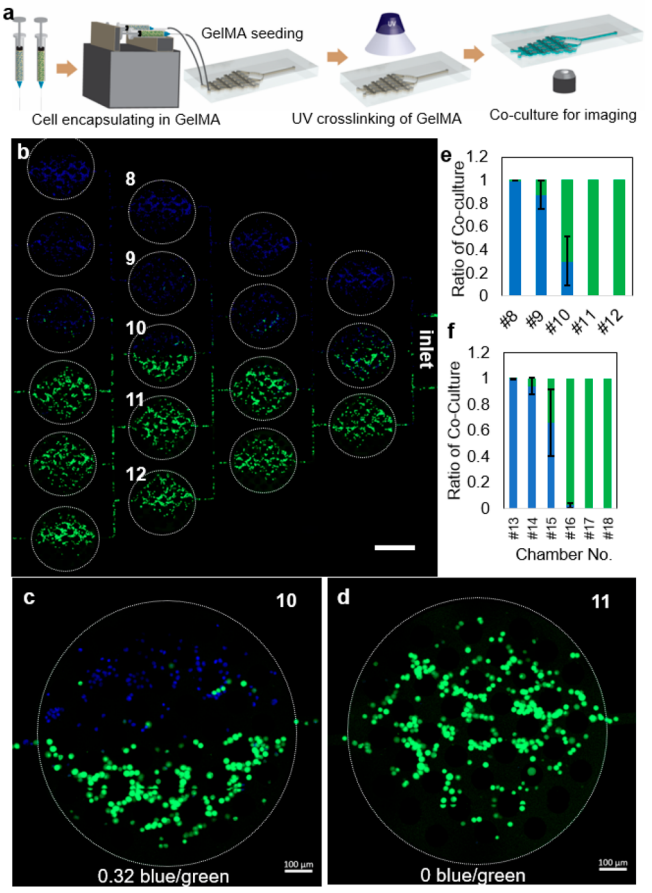

Figure 6. Gradient of 3D-cell encapsulation in hydrogel within the microfluidic device embedded with a micropillar gradient generator. (a) Schematic illustration of the experimental process. (b) Fluorescent image of the gradient of stained cells with 2 different colors of Hoechst and green cell tracker. (c, d) Zoom-in image from the representative chambers 10 and 11, respectively. The empty regions in the circular shape represent the micropillar embedded in the chambers. (e, f) Cell ratio analysis in the third and fourth columns of the chambers of the microfluidic device, respectively. Scale bars: (b) 1000 μm; (c, d) 100 μm.

Figure 6b shows the 3D-cell encapsulation of two types of cells (mutants of cancerous epithelial cells, A431) colored with blue and green inside the microfluidic device, and a clear gradient of cell ratios can be discerned across chambers in the same column. Since the flow rate of the cell mixture from both inlets was the same, microchambers had a symmetric distribution of both types of cells across the center line. As the zoom-in images of Figure 6c,d show, the distribution of the cells within chambers were uniform as compared with experiments carried out in MECT devices (Figure S10b,c), a proof that the micropillars spread the cells evenly within chambers. A clear division of two cell types was visualized from the zoom-in images, as the majority of the cells in green were seeded in the bottom half of chamber 10 (Figure 6c). The distribution of the cells is determined by the velocity profile within the microchambers of each design (Figure S11). A quantitative evaluation of the cell ratios for the last two columns of the device provided clear evidence of the gradient

https://dx.doi.org/10.1021/acsabm.0c00439
ACS Appl. Bio Mater. XXXX, XXX, XXX−XXX

effect as the ratio of blue/green cells drops from 1 to 0 (Figure 6e,f). The MPEM device produces a line contact between two regions of cells. This can be useful in studying the spatiotemporal distribution of cells at the cell−cell contact in different physiological conditions.[57]

This study provides a potential support for coculture systems supplied with chemical gradients. In this capacity, cells can be encapsulated in 3D microenvironments with hydrogels and flowed into the microchambers with a gradient effect. Once cross-linked within the microchambers, cocultures of different cell types and ratios can be used in a wide spectrum of drug screening studies. Microfluidics-based coculture systems have been used to study different cell types, including epithelial and stromal cells for mimicking prostate cancer behavior,[58] breast cancer cells with lung cells,[59] as well as intestine and liver cells.[60] The majority of these studies were focused on 2D coculture of cells. The introduction of 3D coculture with our microchamber system can create a microenvironment that is more physiologically relevant. In addition, the microchambers with the 3D coculture can be peeled off from the top PDMS layer after cell seeding and gel cross-linking. This creates open microchambers where various biological assays can be performed on the coculture of different cell types and ratios. Furthermore, our MPEM and MECT devices could control different ratios of cell concentrations to create cocultures of different numbers of cells.

3. CONCLUSIONS

We have designed a novel microfluidic platform integrating chemical gradient generation and cell culture in a single device. This was achieved by integrating microchambers within a network of microchannels, and potentially with micropillars embedded within the chambers. The microchambers provided spaces for cell seeding and growth and offer a reaction zone for drug screening. We have shown the process for gradient generation and demonstrated the gradient effect in a cancer cell model subject to a chemotherapy agent. The results show the effect of a Dox gradient in the induction of cell death with a clear correlation. Further, we observed and analyzed the synergistic effect of Dox concentrations in the context of fluid shear stress. Finally, these data on cell viability induced in separate chambers at different concentrations of Dox were confirmed with experiments in Petri dishes with corresponding concentrations. Moreover, we showed that this device could potentially provide 3D cell coculturing capacity, paving the way for testing in a 3D microenvironment. Furthermore, this device can be combined with 3D-printers, and the dimensions can scale up which can represent a bioreactor[61] that is capable of analyzing different conditions on the same device. Collectively, these data demonstrate the effectiveness of the device in potentially conducting high-throughput drug screening with a single chip.

4. EXPERIMENTAL SECTION

4.1. Microfluidic Device Fabrication. The fabrication process mainly consists of two steps: the design and fabrication of a silicon mold, and the fabrication of the microfluidic chip. For mold fabrication, a chromium mask coated with a thin layer of SU-8 (Kayaku Advanced Materials, Westborough, MA) was etched using a Laser Writer (Heidelberg DWL-66 FS, Torrance, CA) and an AZ-400 K developer (Microchemicals GmbH, Ulm, Germany) through a chemical reaction. CR-7 chromium etchant (CYANTEK corporation, Fremont, CA) was subsequently used to remove the chromium layer. To ensure that no photoresist remained, a higher concentration (85% water) of AZ-400 K developer was used to dissolve the remaining SU-8. To fabricate the designed features on the Si wafer, S1813 (Microposit, Westborough, MA) positive photoresist was selected for soft lithography. The photoresist was spin coated on the wafer. Then, masked aligned on the top surface of the wafer and DRIE were performed to project the features on the wafer. Then, plasma etching was done to remove the photoresist. The chip is made of polydimethylsiloxane (PDMS) (Sylgard 184, Corning, NY). PDMS was mixed with a curing agent in a 1:10 volume ratio and left in a desiccator for 30 min to degas. The wafer was washed with 99% isopropanol and dried using nitrogen gas. To avoid PDMS adhesion to the wafer, Trichloro (1*H*,1*H*,2*H*,2*H*-perfluorooctyle, silane 97%) (Sigma-Aldrich, St. Louis, MO) was used as the silane agent. The degassed PDMS was poured over the entire mold, and it was again placed inside a desiccator for 30 min to remove any air bubbles formed during pouring. Finally, the wafer was thermally cured inside an oven at 65 °C for 2 h. The PDMS fabrication process is illustrated in a schematic drawing in Figure S12.

4.2. SEM Imaging. The PDMS microfluidic chip without the glass slide was used for SEM imaging. A thermal treatment was applied to the chip in the oven at 50 °C for 30 min before coating to remove excessive humidity and enhance the coating process. Then, a chromium sputter coater (Denton Desk V Sputter) was used to coat a thin layer of chromium on the chip for 15 min. The coated chip was fixed to an SEM holder and then inserted into the SEM (Hitachi S4700 FE). The low-magnification mode with 15 kV was used to image the whole chip for the pillar design and serpentine design with 20× and 25× magnification, respectively. The high-magnification mode with 15 kV was used to image one chamber for the MPEM and MECT with 130× and 67×, respectively.

4.3. Gradient Generation and Analysis. After removing the bubbles from the PDMS chip, blue and yellow dyes were mixed with deionized (DI) water and flowed into the chip with a syringe pump at controlled flow rates and flow rate ratios. After the steady-state is reached, the last column of chambers was imaged in a bright-field mode. The RGB-colored image for each chamber is analyzed to extract the blue color index from the center line of the chamber using a customized MATLAB script.

4.4. COMSOL Simulation. To evaluate the performance of the microchip, a computational fluid dynamics (CFD) simulation was developed using COMSOL Multiphysics. "Creep flow" and "Transport of Diluted Species" physics were used to model the fluid flow, shear stress, and concentration changes in the microfluidic device. For the gradient studies, the inlets have different flow rates to show the effect of flow rate and their ratios on the generated gradient. However, for the shear stress study, both inlets have the same flow rates to study the effect of mechanical stimulation on cell viability. Two flow rates were examined to investigate the effect of flow rate on the shear stress. Shear stress was calculated by adding the following equation to COMSOL analysis: $\tau = \dot{\gamma} \times \mu$, where τ is the shear stress, $\dot{\gamma}$ is the shear rate, and μ is solution viscosity. Shear rate is calculated by the software, and viscosity is the fluid property. We assumed water as the fluid for this simulation.

4.5. Cell Culture. A431 cells (gift from Prof. Kathleen Green, Northwestern University) and A431 cells with GFP tagged E-cadherin (gift from Prof. James K. Wahl, University of Nebraska Medical Center) are cultured in T75 flasks with DMEM-included 10% fetal bovine serum (FBS) and 1% penicillin−streptomycin (10 000 Unit/mL) for 2 days until cells reach confluency. Before the experiment, cell culture media was removed, and the flask was washed with PBS two times. Cells were then trypsinized and suspended for use.

4.6. 3D-Cell Encapsulation. GelMA was used as a hydrogel to encapsulate the cells inside the chambers, and two types of cells were used to demonstrate the coculturing. GelMA was synthesized by following a previous protocol.[55,62,63] Methacrylic anhydride (MA) (Sigma-Aldrich, St. Louis, MO) was mixed with liquid gelatin in PBS at a ratio of 1.25% (v/v). Subsequently, freeze-dried GelMA was dissolved in PBS and combined with a solution of Irgacure 2959 (2-hydroxy-4′-(2-hydroxyethoxy)-2-methyl-propiophenone) (Sigma-Al-

https://dx.doi.org/10.1021/acsabm.0c00439
ACS Appl. Bio Mater. XXXX, XXX, XXX−XXX

drich, St. Louis, MO) and PBS. The final ratio of the photoinitiator (PI) was 0.1%, and the final ratio of the GelMA was 7%.[56] The optimal ratio of the PI was reached by a live/dead study of the cell encapsulation within 7% GelMA cross-linked by different PI ratios (Figure S9 in the Supporting Information).

Mutants of A431 were the cell lines used for 3D coculturing (A431-DPNTP, A431-S2849GDP).[64] Cells were stained with either Hoechst or green cell tracker and mixed with the GelMA solution. The final concentration of cells encapsulated in GelMA solution was around 5 million cells per mL. The GelMA−cell mixture was filled into the 1 mL syringes and flowed into the microchannels with syringe pumps at controlled flow rates. Once a stable condition was reached inside the microchannels, the infusion was stopped, and the GelMA was cured under the UV laser chamber with an intensity of 750 mW for 30 s.

4.7. Cell Seeding for Drug Study. PDMS with a ratio of 1:10 was used to fabricate the microchannels, and it was bonded to glass slides and cured for 30 min at 80 °C inside an oven. Human fibronectin protein (Thermofisher) with a concentration of 50 μg/mL was used to coat the surface of the glass slide as the bottom layer of the microchannels. Fibronectin was flowed into the microchannels by syringes and incubated for 2 h, and the fibronectin-coated microchannel was washed with PBS. A mixture of the cells and DMEM was flowed into the microchannel with syringe pumps at a flow rate of 30 μL/min. The concentration of the cell mixture was about 10 million cells per mL of media. Cell attachment and proliferation inside the microchannel were reached by placing the microchannel inside an incubator for 24 h.

4.8. Drug Testing and Live/Dead Assay. Doxorubicin hydrochloride 98.0−102.0% (HPLC) (Sigma-Aldrich, St. Louis, MO) with a molecular weight of 579.98 was dissolved in water and was diluted in DMEM media. For A431 cells, the live−dead staining kit was diluted with PBS and was continuously flowed into the chambers with cells for 2 h. The live−dead kit contains calcein-AM which stains green to the cytoskeleton of live cells and ethidium homodimer which stains red to the nuclei of dead cells. Cells were then counted with the ImageJ cell counter module. Viability of the cells was calculated as the ratio of the live cells (stained green) over the total number of the cell, summation of the live (green) and dead (red) cells within each chamber.

4.9. Imaging. A ZEISS LSM 800 confocal microscope (4×, 1.4 NA, numerical aperture) was used for live and fixed cell imaging. All images were captured with ZEN software (ZEN, 2017, Zeiss). Bright-field images were taken with a Nikon Ti2 instrument using NIS-Ar software. All image reconstruction and channel alignment were performed using ImageJ software.

4.10. Statistical Analysis. Statistical analyses were performed using the unpaired t test, and statistical significance was determined at $p < 0.05$.

■ ASSOCIATED CONTENT

Supporting Information

The Supporting Information is available free of charge at https://pubs.acs.org/doi/10.1021/acsabm.0c00439.

Gradient generation results, COMSOL simulation, drug screening treatment, zoom-in images, effect of the DMEM flow on morphology, fluorescent images, shear stress distribution, viability test, velocity streamline comparison, and a schematic of the PDMS microfluidic fabrication (PDF)

■ AUTHOR INFORMATION

Corresponding Authors

Ali Tamayol − *Department of Mechanical and Materials Engineering, University of Nebraska, Lincoln, Nebraska 68588, United States; Department of Biomedical Engineering, University of Connecticut, Storrs, Connecticut 06269, United States;* orcid.org/0000-0003-1801-2889; Email: atamayol@unl.edu

Ruiguo Yang − *Department of Mechanical and Materials Engineering, University of Nebraska, Lincoln, Nebraska 68588, United States; Nebraska Center for Integrated Biomolecular Communications (NCIBC), University of Nebraska—Lincoln, Lincoln, Nebraska 68516, United States; Mary & Dick Holland Regenerative Medicine Program, University of Nebraska Medical Center, Omaha, Nebraska 68198, United States;* orcid.org/0000-0002-1361-4277; Email: ryang6@unl.edu

Authors

Arian Jaberi − *Department of Mechanical and Materials Engineering, University of Nebraska, Lincoln, Nebraska 68588, United States*

Amir Monemian Esfahani − *Department of Mechanical and Materials Engineering, University of Nebraska, Lincoln, Nebraska 68588, United States*

Fariba Aghabaglou − *Department of Mechanical and Materials Engineering, University of Nebraska, Lincoln, Nebraska 68588, United States*

Jae Sung Park − *Department of Mechanical and Materials Engineering, University of Nebraska, Lincoln, Nebraska 68588, United States*

Sidy Ndao − *Department of Mechanical and Materials Engineering, University of Nebraska, Lincoln, Nebraska 68588, United States*

Complete contact information is available at: https://pubs.acs.org/10.1021/acsabm.0c00439

Author Contributions

⊥A.J. and A.M.E. contributed equally to this work. A.T., S.N., and R.Y. conceived the idea. A.J., A.M.E., F.A., A.T., and R.Y. analyzed the data. A.J., A.M.E., and F.A. performed the experiments. All the authors were involved in the writing and editing of the manuscript.

Notes

The authors declare no competing financial interest.

■ ACKNOWLEDGMENTS

We acknowledge the funding support: Nebraska Center for Integrated Biomolecular Communication (NCIBC) (NIH National Institutes of General Medical Sciences P20GM113126), National Institutes of Health (GM126831, AR073822), Nebraska Center for Nanomedicine (P30GM127200), the NSF (Award 1826135), and the Nebraska Collaborative Initiative.

■ REFERENCES

(1) Wang, H.; Liu, K.; Chen, K. J.; Lu, Y. J.; Wang, S. T.; Lin, W. Y.; Guo, F.; Kamei, K. I.; Chen, Y. C.; Ohashi, M.; Wang, M. W.; Garcia, M. A.; Zhao, X. Z.; Shen, C. K. F.; Tseng, H. R. A Rapid Pathway Toward a Superb Gene Delivery System: Programming Structural and Functional Diversity into a Supramolecular Nanoparticle Library. *ACS Nano* **2010**, *4* (10), 6235−6243.

(2) Baker, M. A Living System on a Chip. *Nature* **2011**, *471* (7340), 661−665.

(3) Alqurashi, T.; Alnufaili, M.; Hassan, M. U.; Aloufi, S.; Yetisen, A. K.; Butt, H. Laser Inscription of Microfluidic Devices for Biological Assays. *ACS Appl. Mater. Interfaces* **2019**, *11* (13), 12253−12260.

(4) Gao, D.; Li, H. F.; Wang, N. J.; Lin, J. M. Evaluation of the Absorption of Methotrexate on Cells and Its Cytotoxicity Assay by

https://dx.doi.org/10.1021/acsabm.0c00439
ACS Appl. Bio Mater. XXXX, XXX, XXX−XXX

Using an Integrated Microfluidic Device Coupled to a Mass Spectrometer. *Anal. Chem.* **2012**, *84* (21), 9230−9237.
(5) Lu, H.; Koo, L. Y.; Wang, W. M.; Lauffenburger, D. A.; Griffith, L. G.; Jensen, K. F. Microfluidic shear devices for quantitative analysis of cell adhesion. *Anal. Chem.* **2004**, *76* (18), 5257−5264.
(6) Wang, S.-J.; Saadi, W.; Lin, F.; Nguyen, C. M.-C.; Jeon, N. L. Differential effects of EGF gradient profiles on MDA-MB-231 breast cancer cell chemotaxis. *Exp. Cell Res.* **2004**, *300* (1), 180−189.
(7) Shamloo, A.; Ma, N.; Poo, M.-m.; Sohn, L. L.; Heilshorn, S. C. Endothelial cell polarization and chemotaxis in a microfluidic device. *Lab Chip* **2008**, *8* (8), 1292−1299.
(8) Park, J. Y.; Kim, S. K.; Woo, D. H.; Lee, E. J.; Kim, J. H.; Lee, S. H. Differentiation of neural progenitor cells in a microfluidic chip-generated cytokine gradient. *Stem Cells* **2009**, *27* (11), 2646−2654.
(9) Linder, V.; Verpoorte, E.; de Rooij, N. F.; Sigrist, H.; Thormann, W. Application of surface biopassivated disposable poly (dimethylsiloxane)/glass chips to a heterogeneous competitive human serum immunoglobulin G immunoassay with incorporated internal standard. *Electrophoresis* **2002**, *23* (5), 740−749.
(10) Jeon, N. L.; Baskaran, H.; Dertinger, S. K.; Whitesides, G. M.; Van De Water, L.; Toner, M. Neutrophil chemotaxis in linear and complex gradients of interleukin-8 formed in a microfabricated device. *Nat. Biotechnol.* **2002**, *20* (8), 826.
(11) Berg, H. C.; Brown, D. A. Chemotaxis in Escherichia coli analysed by three-dimensional tracking. *Nature* **1972**, *239* (5374), 500−4.
(12) Macnab, R. M.; Koshland, D. E., Jr. The gradient-sensing mechanism in bacterial chemotaxis. *Proc. Natl. Acad. Sci. U. S. A.* **1972**, *69* (9), 2509−12.
(13) Keller, E. F.; Segel, L. A. Model for chemotaxis. *J. Theor. Biol.* **1971**, *30* (2), 225−34.
(14) Jee, A. Y.; Dutta, S.; Cho, Y. K.; Tlusty, T.; Granick, S. Enzyme leaps fuel antichemotaxis. *Proc. Natl. Acad. Sci. U. S. A.* **2018**, *115* (1), 14−18.
(15) Jee, A. Y.; Cho, Y. K.; Granick, S.; Tlusty, T. Catalytic enzymes are active matter. *Proc. Natl. Acad. Sci. U. S. A.* **2018**, *115* (46), E10812−E10821.
(16) Lee, P. J.; Gaige, T. A.; Hung, P. J. Dynamic cell culture: a microfluidic function generator for live cell microscopy. *Lab Chip* **2009**, *9* (1), 164−166.
(17) Zaidon, N.; Nordin, A. N.; Ismail, A. F.; Cheung, M. W. In *Serpentine microfluidic structures for concentration gradient generators*, 2016 Symposium on Design, Test, Integration and Packaging of MEMS/MOEMS (DTIP), 30 May−2 June, 2016; pp 1−5.
(18) Englert, D. L.; Manson, M. D.; Jayaraman, A. Flow-based microfluidic device for quantifying bacterial chemotaxis in stable, competing gradients. *Appl. Environ. Microbiol.* **2009**, *75* (13), 4557−64.
(19) Wolfram, C. J.; Rubloff, G. W.; Luo, X. Perspectives in flow-based microfluidic gradient generators for characterizing bacterial chemotaxis. *Biomicrofluidics* **2016**, *10* (6), 061301.
(20) Kim, S.; Kim, H. J.; Jeon, N. L. Biological applications of microfluidic gradient devices. *Integr Biol-Uk* **2010**, *2* (11−12), 584−603.
(21) Chung, B. G.; Flanagan, L. A.; Rhee, S. W.; Schwartz, P. H.; Lee, A. P.; Monuki, E. S.; Jeon, N. L. Human neural stem cell growth and differentiation in a gradient-generating microfluidic device. *Lab Chip* **2005**, *5* (4), 401−6.
(22) Ruan, J.; Wang, L.; Xu, M.; Cui, D.; Zhou, X.; Liu, D. Fabrication of a microfluidic chip containing dam, weirs and gradient generator for studying cellular response to chemical modulation. *Mater. Sci. Eng., C* **2009**, *29* (3), 674−679.
(23) Lim, W.; Park, S. A microfluidic spheroid culture device with a concentration gradient generator for high-throughput screening of drug efficacy. *Molecules* **2018**, *23* (12), 3355.
(24) Liu, X.-J.; Hu, S.-W.; Xu, B.-Y.; Zhao, G.; Li, X.; Xie, F.-W.; Xu, J.-J.; Chen, H.-Y. Microfluidic liquid-air dual-gradient chip for synergic effect bio-evaluation of air pollutant. *Talanta* **2018**, *182*, 202−209.
(25) Abdulla, A.; Liu, W.; Gholamipour-Shirazi, A.; Sun, J.; Ding, X. High-Throughput Isolation of Circulating Tumor Cells Using Cascaded Inertial Focusing Microfluidic Channel. *Anal. Chem.* **2018**, *90* (7), 4397−4405.
(26) Li, L.; Wang, W.; Ding, M.; Luo, G.; Liang, Q. Single-Cell-Arrayed Agarose Chip for in Situ Analysis of Cytotoxicity and Genotoxicity of DNA Cross-Linking Agents. *Anal. Chem.* **2016**, *88* (13), 6734−6742.
(27) Lee, M.; Lee, K.; Kim, K. H.; Oh, K. W.; Choo, J. SERS-based immunoassay using a gold array-embedded gradient microfluidic chip. *Lab Chip* **2012**, *12* (19), 3720−3727.
(28) Shemesh, J.; Jalilian, I.; Shi, A.; Heng Yeoh, G.; Knothe Tate, M. L.; Ebrahimi Warkiani, M. Flow-induced stress on adherent cells in microfluidic devices. *Lab Chip* **2015**, *15* (21), 4114−4127.
(29) Yankaskas, C. L.; Thompson, K. N.; Paul, C. D.; Vitolo, M. I.; Mistriotis, P.; Mahendra, A.; Bajpai, V. K.; Shea, D. J.; Manto, K. M.; Chai, A. C.; Varadarajan, N.; Kontrogianni-Konstantopoulos, A.; Martin, S. S.; Konstantopoulos, K. A microfluidic assay for the quantification of the metastatic propensity of breast cancer specimens. *Nature Biomedical Engineering* **2019**, *3* (6), 452−465.
(30) Han, J.; Lim, W.; You, D.; Jeong, Y.; Kim, S.; Lee, J. E.; Shin, T. H.; Lee, G.; Park, S. Chemoresistance in the Human Triple-Negative Breast Cancer Cell Line MDA-MB-231 Induced by Doxorubicin Gradient Is Associated with Epigenetic Alterations in Histone Deacetylase. *J. Oncol.* **2019**, *2019*, 12.
(31) Lee, H. J.; Diaz, M. F.; Price, K. M.; Ozuna, J. A.; Zhang, S.; Sevick-Muraca, E. M.; Hagan, J. P.; Wenzel, P. L. Fluid shear stress activates YAP1 to promote cancer cell motility. *Nat. Commun.* **2017**, *8* (1), 14122.
(32) Polacheck, W. J.; German, A. E.; Mammoto, A.; Ingber, D. E.; Kamm, R. D. Mechanotransduction of fluid stresses governs 3D cell migration. *Proc. Natl. Acad. Sci. U. S. A.* **2014**, *111* (7), 2447.
(33) Regmi, S.; Fu, A.; Luo, K. Q. High Shear Stresses under Exercise Condition Destroy Circulating Tumor Cells in a Microfluidic System. *Sci. Rep.* **2017**, *7* (1), 39975.
(34) Xiong, N.; Li, S.; Tang, K.; Bai, H.; Peng, Y.; Yang, H.; Wu, C.; Liu, Y. Involvement of caveolin-1 in low shear stress-induced breast cancer cell motility and adhesion: Roles of FAK/Src and ROCK/p-MLC pathways. *Biochim. Biophys. Acta, Mol. Cell Res.* **2017**, *1864* (1), 12−22.
(35) Rizvi, I.; Gurkan, U. A.; Tasoglu, S.; Alagic, N.; Celli, J. P.; Mensah, L. B.; Mai, Z.; Demirci, U.; Hasan, T. Flow induces epithelial-mesenchymal transition, cellular heterogeneity and biomarker modulation in 3D ovarian cancer nodules. *Proc. Natl. Acad. Sci. U. S. A.* **2013**, *110* (22), E1974.
(36) Anand, P.; Fu, A.; Teoh, S. H.; Luo, K. Q. Application of a fluorescence resonance energy transfer (FRET)-based biosensor for detection of drug-induced apoptosis in a 3D breast tumor model. *Biotechnol. Bioeng.* **2015**, *112* (8), 1673−1682.
(37) Triantafillu, U. L.; Park, S.; Kim, Y. Fluid Shear Stress Induces Drug Resistance to Doxorubicin and Paclitaxel in the Breast Cancer Cell Line MCF7. *Advanced Therapeutics* **2019**, *2* (3), 1800112.
(38) Lee, M.; Lee, K.; Kim, K. H.; Oh, K. W.; Choo, J. SERS-based immunoassay using a gold array-embedded gradient microfluidic chip. *Lab Chip* **2012**, *12*, 3720.
(39) Park, J. Y.; Yoo, S. J.; Hwang, C. M.; Lee, S.-H. Simultaneous generation of chemical concentration and mechanical shear stress gradients using microfluidic osmotic flow comparable to interstitial flow. *Lab Chip* **2009**, *9* (15), 2194−2202.
(40) Toh, Y.-C.; Voldman, J. Fluid shear stress primes mouse embryonic stem cells for differentiation in a self-renewing environment via heparan sulfate proteoglycans transduction. *FASEB J.* **2011**, *25* (4), 1208−1217.
(41) Chatterjee, K.; Zhang, J.; Honbo, N.; Karliner, J. S. Doxorubicin Cardiomyopathy. *Cardiology* **2010**, *115* (2), 155−162.
(42) Shang, M.; Soon, R. H.; Lim, C. T.; Khoo, B. L.; Han, J. Microfluidic modelling of the tumor microenvironment for anti-cancer drug development. *Lab Chip* **2019**, *19* (3), 369−386.

https://dx.doi.org/10.1021/acsabm.0c00439
ACS Appl. Bio Mater. XXXX, XXX, XXX−XXX

(43) Sugiura, S.; Hattori, K.; Kanamori, T. Microfluidic Serial Dilution Cell-Based Assay for Analyzing Drug Dose Response over a Wide Concentration Range. *Anal. Chem.* **2010**, *82* (19), 8278−8282.
(44) Germain, T.; Ansari, M.; Pappas, D. Observation of reversible, rapid changes in drug susceptibility of hypoxic tumor cells in a microfluidic device. *Anal. Chim. Acta* **2016**, *936*, 179−84.
(45) Li, L.; Li, Y.; Shao, Z.; Luo, G.; Ding, M.; Liang, Q. Simultaneous Assay of Oxygen-Dependent Cytotoxicity and Genotoxicity of Anticancer Drugs on an Integrated Microchip. *Anal. Chem.* **2018**, *90* (20), 11899−11907.
(46) Peng, C.-C.; Liao, W.-H.; Chen, Y.-H.; Wu, C.-Y.; Tung, Y.-C. A microfluidic cell culture array with various oxygen tensions. *Lab Chip* **2013**, *13* (16), 3239−3245.
(47) Castiaux, A. D.; Spence, D. M.; Martin, R. S. Review of 3D cell culture with analysis in microfluidic systems. *Anal. Methods* **2019**, *11* (33), 4220−4232.
(48) Duval, K.; Grover, H.; Han, L. H.; Mou, Y.; Pegoraro, A. F.; Fredberg, J.; Chen, Z. Modeling Physiological Events in 2D vs. 3D Cell Culture. *Physiology* **2017**, *32* (4), 266−277.
(49) Caliari, S. R.; Burdick, J. A. A practical guide to hydrogels for cell culture. *Nat. Methods* **2016**, *13* (5), 405−414.
(50) Wallin, P.; Zanden, C.; Carlberg, B.; Hellstrom Erkenstam, N.; Liu, J.; Gold, J. A method to integrate patterned electrospun fibers with microfluidic systems to generate complex microenvironments for cell culture applications. *Biomicrofluidics* **2012**, *6* (2), 24131.
(51) Frey, O.; Misun, P. M.; Fluri, D. A.; Hengstler, J. G.; Hierlemann, A. Reconfigurable microfluidic hanging drop network for multi-tissue interaction and analysis. *Nat. Commun.* **2014**, *5*, 4250.
(52) Chen, C. P.; Townsend, A. D.; Hayter, E. A.; Birk, H. M.; Sell, S. A.; Martin, R. S. Insert-based microfluidics for 3D cell culture with analysis. *Anal. Bioanal. Chem.* **2018**, *410* (12), 3025−3035.
(53) Ghorbanian, S.; Qasaimeh, M. A.; Akbari, M.; Tamayol, A.; Juncker, D. Microfluidic direct writer with integrated declogging mechanism for fabricating cell-laden hydrogel constructs. *Biomed. Microdevices* **2014**, *16* (3), 387−395.
(54) Kang, E.; Jeong, G. S.; Choi, Y. Y.; Lee, K. H.; Khademhosseini, A.; Lee, S.-H. Digitally tunable physicochemical coding of material composition and topography in continuous microfibres. *Nat. Mater.* **2011**, *10* (11), 877−883.
(55) Rezaei Nejad, H.; Goli Malekabadi, Z.; Kazemzadeh Narbat, M.; Annabi, N.; Mostafalu, P.; Tarlan, F.; Zhang, Y. S.; Hoorfar, M.; Tamayol, A.; Khademhosseini, A. Laterally Confined Microfluidic Patterning of Cells for Engineering Spatially Defined Vascularization. *Small* **2016**, *12* (37), 5132−5139.
(56) Russell, C. S.; Mostafavi, A.; Quint, J. P.; Panayi, A. C.; Baldino, K.; Williams, T. J.; Daubendiek, J. G.; Hugo Sánchez, V.; Bonick, Z.; Trujillo-Miranda, M.; Shin, S. R.; Pourquie, O.; Salehi, S.; Sinha, I.; Tamayol, A. In Situ Printing of Adhesive Hydrogel Scaffolds for the Treatment of Skeletal Muscle Injuries. *ACS Applied Bio Materials* **2020**, *3* (3), 1568−1579.
(57) Bogdanowicz, D. R.; Lu, H. H. Multifunction co-culture model for evaluating cell-cell interactions. *Methods Mol. Biol.* **2013**, *1202*, 29−36.
(58) Ivich, F.; Tran, M.; Tahsin, S.; Frank, S. B.; Kraft, A.; Miranti, C. K.; Zohar, Y.; Jiang, L. Application of a Microfluidic-Based Model of a Human Prostate Gland for Cancer Research. *2018 IEEE 12th International Conference on Nano/Molecular Medicine and Engineering (NANOMED)* **2018**, 109−112.
(59) Yuan, T.; Gao, D.; Li, S.; Jiang, Y. Co-culture of tumor spheroids and monocytes in a collagen matrix-embedded microfluidic device to study the migration of breast cancer cells. *Chin. Chem. Lett.* **2019**, *30* (2), 331−336.
(60) Jie, M.; Li, H.-F.; Lin, L.; Zhang, J.; Lin, J.-M. Integrated microfluidic system for cell co-culture and simulation of drug metabolism. *RSC Adv.* **2016**, *6* (59), 54564−54572.
(61) Bhise, N. S.; Manoharan, V.; Massa, S.; Tamayol, A.; Ghaderi, M.; Miscuglio, M.; Lang, Q.; Shrike Zhang, Y.; Shin, S. R.; Calzone, G.; Annabi, N.; Shupe, T. D.; Bishop, C. E.; Atala, A.; Dokmeci, M. R.; Khademhosseini, A. A liver-on-a-chip platform with bioprinted hepatic spheroids. *Biofabrication* **2016**, *8* (1), 014101.
(62) Tamayol, A.; Najafabadi, A. H.; Aliakbarian, B.; Arab-Tehrany, E.; Akbari, M.; Annabi, N.; Juncker, D.; Khademhosseini, A. Hydrogel Templates for Rapid Manufacturing of Bioactive Fibers and 3D Constructs. *Advanced Healthcare. Adv. Healthcare Mater.* **2015**, *4* (14), 2146−2153.
(63) Yue, K.; Trujillo-de Santiago, G.; Alvarez, M. M.; Tamayol, A.; Annabi, N.; Khademhosseini, A. Synthesis, properties, and biomedical applications of gelatin methacryloyl (GelMA) hydrogels. *Biomaterials* **2015**, *73*, 254−271.
(64) Broussard, J. A.; Yang, R.; Huang, C.; Nathamgari, S. S. P.; Beese, A. M.; Godsel, L. M.; Hegazy, M. H.; Lee, S.; Zhou, F.; Sniadecki, N. J.; Green, K. J.; Espinosa, H. D. The desmoplakin-intermediate filament linkage regulates cell mechanics. *Mol. Biol. Cell* **2017**, *28* (23), 3156−3164.

https://dx.doi.org/10.1021/acsabm.0c00439
ACS Appl. Bio Mater. XXXX, XXX, XXX−XXX